Generation and Control of Sound Bullets with a Nonlinear Acoustic Lens

Alessandro Spadoni [*], **Chiara Daraio** [*] [†]

[*]Graduate Aerospace Laboratories (GALCIT), and [†]Applied Physics, California Institute of Technology, Pasadena, CA 91125

Submitted to Proceedings of the National Academy of Sciences of the United States of America

Acoustic lenses are employed in a variety of applications, from biomedical imaging [1, 2] and surgery [3] to defense systems [4] and damage detection in materials [5]. Focused acoustic signals, for example, enable ultrasonic transducers to image the interior of the human body [1, 2]. But currently the performance of acoustic devices is limited by their linear operational envelope, which implies relatively inaccurate focusing and low focal power. Here we show a dramatic focusing effect and the generation of compact acoustic pulses (sound bullets) in solid and fluid media, with energies orders of magnitude greater than previously achievable. This focusing is made possible by a tunable, nonlinear acoustic lens, which consists of ordered arrays of granular chains. The amplitude, size, and location of the sound bullets can be controlled by varying the static pre-compression of the chains. Theory and numerical simulations demonstrate the focusing effect, and photoelasticity experiments corroborate it. Our nonlinear lens permits a qualitatively new way of generating high-energy acoustic pulses, which may improve imaging capabilities through increased accuracy and signal-to-noise ratios and may lead to more effective non-intrusive scalpels, for example, for cancer treatment [3, 6, 7].

The focusing of acoustic waves at a desired location is usually realized with electromechanical transducers and methods such as geometric focusing [5], time-reversal focusing [8], or beamforming via phase lags [3, 9, 10]. In geometric focusing, the transducers' geometry is exploited to focus signals. In time reversal and beamforming methods, appropriate phase delays among acoustic signals are used to focus them in a desired region. Each method is limited by its reliance on actuators, which are incapable of generating compact, non-oscillatory, and high-amplitude signals, typically resulting in cumbersome and application-specific devices. Recently, acoustic metamaterials [11] as well as superlenses [12] and hyperlenses [13] aimed at improving spatial resolution have been introduced. However, their continued reliance on linear wave dynamics limits their spatial accuracy, energy intensity, and dynamic focus control.

Here we introduce an acoustic lens that uses nonlinear wave dynamics to accurately focus high-amplitude acoustic signals, achieving a transient focal region of higher energy density than previously possible. The position, amplitude, and frequency content of the focal region in an adjacent solid or fluid host medium are dynamically controllable. The acoustic lens consists of an array of nonlinear transducers based on discrete power-law materials (e.g., chains of spherical particles) (Fig. 1A). In contrast to linear elastic materials in which force F and deformation δ obey the relation $F = k_L\delta$, with stiffness constant k_L, discrete power-law materials do not support tensile forces and feature an unusual behavior described by $F = k_N\delta^n$, with stiffness constant k_N and power-law exponent $n > 1$. The nonlinearity of the force-deformation relation makes discrete power-law materials a host for compact acoustic waves, which are stable and have easily controllable behavior [14, 15, 16, 17, 18]. We take advantage of these characteristics to modify incoming acoustic waves into compact, high-amplitude pulses within the lens (see insets in Fig. 1A). These pulses can subsequently be focused in an adjacent fluid or solid host medium.

Power-law materials such as arrays of spherical particles can support linear, weakly nonlinear, and highly nonlinear wave dynamics, depending on the initial strain state of the material, which can be controlled by a static pre-compression force F_0 (Fig. 1B) [14]. For incoming signals leading to low particle interaction forces F_m such that $F_m \ll F_0$, the resulting wave field is linear. If $F_m \approx F_0$, the wave field is characterized by the classic weakly nonlinear soliton solutions of the Korteweg-De Vries (KDV) equation [14, 19], whose phase velocity V_s depends on wavelength and amplitude [20]. The weakly nonlinear regime is depicted as the gray shaded area in Fig. 1B.

If $F_m \gg F_0$, the wave field is highly nonlinear: no linear spatial derivatives are present in the governing equation in the continuum limit [14]. The wave field consists of combinations of compact solitary waves, whose wavelength is constant (approximately five sphere diameters) and whose phase velocity depends on their amplitude [14, 15]. Short input signals lead to a single solitary wave; longer inputs lead to a train of solitary waves or shock-like structures (see insets in Fig. 1A) [14, 21, 22]. All three waveforms travel with a phase velocity V_s that depends on the maximum dynamic force F_m and the static pre-compression force F_0 [14, 18, 23]. The frequency content of the wave field is proportional to k_sV_s, with a wavenumber k_s that depends on properties of the power-law material [14]. The frequency content can be controlled by controlling V_s through F_0. Here we use chains of spheres as a simple representation of a nonlinear medium with constitutive-law exponent $n = 3/2$ [14, 15, 24].

We designed a nonlinear acoustic lens by assembling chains of spheres into an array. The individual chains in the array were pre-compressed differentially such that an acoustic signal with fixed phase incident on the lens results in transmitted waves with phase delays. The pre-compression and phase delays were chosen so that the individual waves transmitted by each chain coalesce at a focal point in the adjacent host medium (Fig. 1C). For an impulsive input to the lens, Fig. 2 illustrates the phase delays (Fig. 2A), transmitted waves shortly after their generation (Fig. 2B), and the focusing of the acoustic energy in the host medium, with a symmetric pressure distribution with one maximum and one minimum (Fig. 2C). These are obtained from analytical calculations with air as the host medium (see Eqs. [S1]–[S3] in the Supporting Information). The acoustic energy in the host medium is focused into a "sound bullet"— a traveling,

Reserved for Publication Footnotes

compact region of high energy density. Sound bullets result from the coalescence of acoustic waves, which have frequencies in the audible range for the lens parameters we chose. The individual waves transmitted by the nonlinear acoustic lens are compact. They consist of a single wave crest for an input of short duration. This characteristic of the transmitted waves leads to the compact nature and accurate focusing of sound bullets. In contrast to optical bullets that are theorized to reside in optically dispersive media [25, 26], sound bullets arise when solitary waves created within a nonlinear granular medium coalesce in a linear non-dispersive medium. This makes sound bullets feasible in a variety of host media.

The analytical calculations on which Fig. 2 is based assume perfectly circular wave fronts radiating from an idealized interface between the lens and the host medium. To test to what extent the analytical results carry over to a more realistic setting, we use numerical simulations with a fluid-structure-interaction (FSI), finite-element (FE) model coupled to a discrete-particle (DP) model (see Supporting Information). The simulated acoustic lens is identical to the prototype illustrated in Fig. 1A, with an incident pulse generated by impact with a conformal striker. For a striker with an impact velocity of $1\,\mathrm{m\,s^{-1}}$ and a mass equal to that of 21 spheres, the resulting pressure field in air for a focal point ($x_f = 9$ cm, $y_f = 7$ cm) is shown in Fig. 3A, along with the required time delay. The sound bullet, formed off axis because of the selected asymmetric pre-compression schedule, attains a maximum pressure $p_B \approx 79$ Pa, corresponding to 38 dB (dB $= 20\log_{10}(p/p_0)$, with a reference pressure $p_0 = 1$ Pa [27]). The pressure distribution at the focal point agrees qualitatively with that predicted analytically (see Eq. [3] in Materials and Methods) in that both the wavelength and double-peaked shape agree (inset in Fig. 3A).

Because the sound bullet is a superposition of compact waves, it propagates in the vicinity of the focal point at the speed of sound of the host medium, as long as the individual compact waves that comprise the sound bullet interfere constructively. The distance over which this is the case depends on the curvature of the phase delay distribution and hence is controllable, along with the focal length, by the static pre-compression. In the numerical simulations, the distance traveled is evident in the root-mean-square (RMS) pressure field and is on the order of the focal length (Fig. 3B). If we vary the focal length by varying the pre-compression, we can also obtain, for example at zero or uniform pre-compression, a focal point at infinity, or a compact planar wavefront (Fig. 3C).

The generation of stable and compact solitary waveforms seen in these results arises because nonlinearity and dispersion balance in the lens [14, 15]. The stability and compactness are retained even if the input amplitude is increased, making it possible to produce arbitrarily large signals within the lens as long as the force-deformation power law is unaltered. As a consequence, the pressure amplitude of sound bullets generated with our lens increases as the impact velocity v_0 increases. For example, with $v_0 = 4\,\mathrm{m\,s^{-1}}$, the resulting sound bullet attains a pressure amplitude of 675 Pa, corresponding to 57 dB—two orders of magnitude greater than what is achievable with linear acoustic lenses [1, 2, 4, 5, 11, 27].

To corroborate our analytical and numerical results, we performed experiments to demonstrate the focusing of pressure waves in a solid host medium (a polycarbonate plate) (Fig. 4A). To compare with the experimental results, we extended the analytical calculations and the numerical DP/FE simulations to account for stresses and strains in solids (see Supporting Information). The DP/FE model suggests that the large striker mass (longer contact duration) used in the experiments leads to shock-like waves propagating within the lens (Fig. 4B), in place of the single solitary wave generated with a small striker mass (shorter contact duration) (Fig. 1A). We chose the pre-compression (Fig. S3D) to obtain a focal point in the polycarbonate plate 10 cm from the lens' edge on its symmetry axis (Fig. 4A), and we visualized the focused waves in the experiments by measuring photoelastic fringes in the polycarbonate plate. The photoelastic fringes produced by the dynamic stress in the plate were captured with a black-and-white high-speed camera and compared to the DP/FE model. The numerical simulations indicated that the stress along the symmetry axis at the focal point has a shock-like profile (Fig. 4C), and this was used to guide the image acquisition system. The numerically simulated photoelastic stress fringes agree qualitatively with those obtained experimentally (Fig. 4D). Subtle misalignment of the striker, spheres, and mid-plane of the plate produced other wave modes that affect the experimentally measured photoelastic fringes. Nonetheless, a clear stress concentration is observed, reaching the focal point only $\approx 5\%$ later in the experiments than in the numerical simulation (Fig. 4D).

The nonlinear acoustic lens provides a more compact focal region than is achievable with an array of linear sources, especially when operating in the transient regime (e.g., generating single sound bullets). These improvements stem from the non-oscillatory and compact nature of signals transmitted by our lens (see Eq. [1] in Materials and Methods), which is not achievable with traditional linear devices. It is possible that our lens design may be further improved by employing nonlinear media with a higher constitutive-law exponent n, as the wavelength of solitary waves scales as $\lambda = \pi a[\sqrt{n(n+1)/6}]/(n-1)$ [14] with a as the particle size, so that greater n may lead to a sharper focus.

The nonlinear lens expands the capabilities of existing acoustic transducers. The chains of particles composing the lens transform a given incident acoustic signal into either a single pulse or trains of pulses (compact solitary waves), which are tunable by mechanical means. The phase velocity of the waves within the lens can be controlled by adjusting the static pre-compression of each chain, while the wavelength is determined by the size of the particles. These characteristics allow the focusing of waves transmitted into a solid or fluid host medium and the generation of compact sound bullets of arbitrarily large amplitudes (here we demonstrated up to 57 dB amplification at the focus). Sound bullets can travel finite distances in the host medium while retaining their compact shape. Such compact, transient pressure pulses were not achievable with previously available technologies, which only allow oscillatory signals. The acoustic lens can also be used as an effective filter, capable of controlling the frequency content of the pressure field in the focal region by controlling the pre-compression. Acoustic lenses like the one we demonstrated have the potential to dramatically impact a variety of applications, such as biomedical devices, non-destructive evaluation, and defense systems. For example, sound bullets may conceivably be used as a non-invasive scalpel to accurately target tumors in hyperthermia applications.

Materials and Methods

Analytical Model. In the continuum limit (long wavelength compared to the sphere diameter), the solitary waves are thought to have the compact structure (cf. ref. [14])

$$u_n(t) = \begin{cases} A_n \cos^4 \alpha_n & \alpha_n \in [-\pi/2, \pi/2], \\ 0 & \text{otherwise}, \end{cases} \qquad \textbf{[1]}$$

with argument

$$\alpha_n = k_s \left[x - V_{s,n}(t - \Delta t_n) \right]. \quad \textbf{[2]}$$

Here, u is the displacement of a material point, and x and t are the spatial and temporal coordinates. For a given particle size, the wavenumber k_s is a constant, i.e. $k_s = \sqrt{10}/(5D)$ [14]. The index n indicates a particular chain of spheres wtihin the lens.

In our theoretical analysis, we consider the focusing properties of the nonlinear acoustic lens in solid and fluid host media, limiting the study to the case $F_m \gg F_0$. The interactions between the individual granular chains and the host medium are assumed to be contact interactions of solid spheres with either a solid half space or thin metal plates separating the spheres themselves from a fluid half space. In both cases, we assume the mechanical disturbances to be perceived as point sources by the linear isotropic host medium. Geometric or ray acoustics [20] can then be used to estimate the phase delay distribution Δt_n necessary to focus energy at a desired location (x_f, y_f) (Eqs. [**S1**]–[**S3**] in the Supporting Information).

In the case of a fluid host medium, assuming that the displacement of each thin metal plate is represented by the same function as that describing a solitary wave (Eq. **[1]**) with amplitude A_n, yields the pressure field (Eqs. [**S4**]-[**S9**] in the Supporting Information)

$$p(x,y,t) = \frac{\rho c k_s V_{s,n} a}{2} \sum_{n=1}^{N} \frac{A_n \left[2\sin\left(2k_s\phi_n\right) + \sin\left(4k_s\phi_n\right) \right]}{r_n}. \quad \textbf{[3]}$$

This pressure field is nonzero only where $k_s\phi_n \in [-\pi/2, \pi/2]$; it is zero otherwise. Here ρ is the density of the host medium, c is the linear speed of sound in the host medium, and the factor a is a small coordinate shift to avoid singularities in the linear solution at the lens–host medium interface. Because the pressure amplitude cannot easily be obtained analytically, we fix one constant $aA_n = \text{const}$ in Eq. **[3]** to match numerical simulations. In Eq. **[3]**, N is the number of chains composing the lens, $r_n = \sqrt{(x - x_n)^2 + (y - y_n)^2}$, and $\phi_n = V_{s,n}\left(r_n/c - a/c - t + \Delta t_n\right)$.

Numerical Model. The FSI model is employed to evaluate the interaction of moving thin metal plates and the fluid host medium. Both air and the particles in the lens are assumed initially at rest, and, for simplicity, the pressure at the boundaries is assumed zero (corresponding to assuming the fluid to be confined to a closed box); this explains the reverberation seen in Fig. 3A. The DP model treats each sphere as a point mass, and the contact between any two spheres is represented as a spring of stiffness determined by Hertz contact theory [14, 15, 16, 17, 18, 24].

Experimental Methods. The experimental prototype of the acoustic lens (Fig. 1A) is made of Aluminum 6061-T051 and measures $30.5 \times 23 \times 7.6$ cm. It accommodates 21 chains each composed of 21 stainless steel spheres (properties listed in Table S1 in the Supporting Information). Each chain was independently statically pre-compressed by a different force F_0, and the chains were separated from each other with stainless steel shim stock of thickness 0.15 mm. The inside surfaces of the lens casing were lined with Teflon sheets to minimize friction. The front and back sides of the lens casing feature slots (Fig. S3A in the Supporting Information) to accommodate individual strands of fishing line used to pre-compress each chain. The topmost sphere of each chain was threaded with fishing line, and was secured to one side of the lens casing, to which weights were connected. Water bottles with variable water content were used as they provided the necessary resolution in setting the pre-compression weights (see Figs. S3C and S3D in the Supporting Information for the required time delay and associated pre-compression forces). The assembled lens was set vertically on a polycarbonate plate (Table S2 in the Supporting Information) of dimension $25 \times 25 \times 1.9$ cm, which in turn rested on a table (Fig. S3A).

Upon applying the differential pre-compression, the lengths of the chains differed, posing a challenge in imparting mechanical energy to all chains simultaneously. The adopted solution consisted of drilling holes in the first sphere of each chain to accommodate a 2.5-cm long screw. The impacting plate was modified by adding 21 holes (2.5 cm in depth, 1 cm in diameter) to accommodate the screws protruding from each sphere. The holes were then filled with a two-part CASTAMOUNT acrylic resin from Pace technologies. In this manner, the contact edge of the striker plate aligned with the top portion of each chain (Fig. S3A in the Supporting Information). Finally, the camera was triggered using a PCB accelerometer placed on the top portion of the striker assembly.

With the DP/FE model as guidance, a Vision Research, Phantom V12 high-speed camera was triggered $280\,\mu$s after impact. The black-and-white camera was set to acquire images at $300,000$ samples per second, plus a reference image (25×10 cm) of the polycarbonate plate at rest (Fig. S3B in the Supporting Information). To remove the shadows of the fishing line and to enhance the visible photoelastic fringes, the reference image was subtracted from each acquired frame.

ACKNOWLEDGMENTS. The authors thank Vitali F. Nesterenko for initial discussions, Tapio Schneider for helpful suggestions and Veronica Eliasson for valuable experimental insight. Funding from ARO (Grant Number 54272-EG), NSF (MRSEC at Caltech and NSF-CMMI-0806762-CAREER) is also acknowledged.

1. M. Fatemi and J. F. Greenleaf. Ultrasound-stimulated vibro-acoustic spectrography. Science, 280(5360):82, 1998.
2. D. S. Kim, A. P. Dhawan, H. K. Huang. Principles and Advanced Methods in Medical Imaging and Image Analysis. World Scientific, Hackensack, NJ, 2008.
3. E. S. Ebbini. Multiple-focus ultrasound phased-array pattern synthesis - optimal driving-signal distributions for hyperthermia. IEEE Transactions on Ultrasonics Ferroelectrics and Frequency Control, 36(5):540–548, 1989.
4. J. M. Buckingham, V. B. Berknout, and S. A. L. Glegg. Imaging the ocean with ambient noise. Nature, 356:327–329, 1992.
5. J. Kushibiki and N. Chubachi. Material characterization by line-focus-beam acoustic microscope. IEEE Transactions on Sonics and Ultrasonics, 32(2):189–212, 1985.
6. J. A. Dickson and S. K. Calderwood. In vivo hyperthermia of yoshida tumour induces entry of non-proliferating cells into cycle. Nature, 263:772–774, 1976.
7. Y. G. Shellman, W. R. Howe, L. A. Miller, N. B. Goldstein, T. R. Pacheco, R. L. Mahajan, S. M. LaRue, and D. A. Norris. Hyperthermia induces endoplasmic reticulum-mediated apoptosis in melanoma and non-melanoma skin cancer cells. Journal of Investigative Dermatology, 128(4):949–956, 2007.
8. M. Fink. Time-reversal of ultrasonic fields 1. basic principles. IEEE Transactions on Ultrasonics Ferroelectrics and Frequency Control, 39(5):555–566, 1992.
9. D. E. Dudgeon. Array Signal Processing: Concepts and Techniques. Prentice-Hall, Upper Saddle River, NJ, 1993.
10. K. D. Van Veen and K. M. Buckley. Beamforming: a versatile approach to spatial filtering. IEEE ASSP Magazine, 5(2):4–24, 1988.
11. A. Håkansson, F. Cervera and J. Sánchez-Dehesa. Sound focusing by flat acoustic lenses without negative refraction. Applied Physics Letters, 86, 054102, 2005.
12. X. Zhang and Z. Liu. Superlenses to overcome the diffraction limit. Nature Materials, 7:435–441, 2008.
13. J. Li, L. Fok, X. Yin, G. Bartal and X. Zhang. Experimental demonstration of an acoustic magnifying hyperlens. Nature Materials, 8:931–934, 2009.
14. V. F. Nesterenko. Dynamics of heterogeneous materials. Springer-Verlag, New York, NY, 2001.
15. V. F. Nesterenko. Propagation of nonlinear compression pulses in granular media. Journal of Applied Mechanics and Technical Physics, 24(5):733–43, 1983.
16. M. A. Porter, C. Daraio, I. Szelengowicz, E. B. Herbold, and P. G. Kevrekidis. Highly nonlinear solitary waves in heterogeneous periodic granular media. Physica D-Nonlinear Phenomena, 238(6):666–676, 2009.
17. S. Sen, J. Hong, J. Bang, E. Avalos and R. Doney. Solitary waves in the granular chain. Physics Reports-Review Section of Physics Letters, 462(2):21–66, 2008.
18. C. Daraio, V. F. Nesterenko, E. B. Herbold, and S. Jin. Tunability of solitary wave properties in one-dimensional strongly nonlinear phononic crystals. Physical Review E, 73(2), 2006.
19. D. J. Korteweg and G. De Vries. On the change of form of long waves advancing in a rectangular canal, and on a new type of long stationary waves. Phil. Mag, 39(5):422–443, 1895.
20. G. B. Witham. Linear and nonlinear waves. Wiley Interscience, New York, NY, 1999.
21. A. Shukla, M. H. Sadd and Q. M. Tai. Influence of loading pulse duration on dynamic load transfer in a simulated granular medium. Journal of the Mechanics and Physics of Solids, 41(11):1795–1808, 1993.
22. Y. Zhu, F. Sienkiewicz, A. Shukla and M. H. Sadd. A comparison of explosively generated pulse propagation in assemblies of disks and spheres. Journal of Engineering Mechanics, 123(10):1050–1059, 1997.
23. C. Coste and B. Gilles. On the validity of hertz contact law for granular material acoustics. European Physical Journal B, 7(1):155–168, 1999.
24. K. L. Johnson. Contact mechanics. Cambridge University Press, Cambridge, UK, 2003.
25. Y. Silberberg. Collapse of optical bullets. Optics Letters, 15(22): 1282–1284, 1990.
26. S. A. Ponomarenko and G. P. Agrawal. Linear optical bullets. Physical Review E, 73(2), 2006.
27. A. Håkansson, J. Sánchez-Dehesa and L. Sanchis. Acoustic lens design by genetic algorithms. Physical Review B, 70, 214302, 2004.

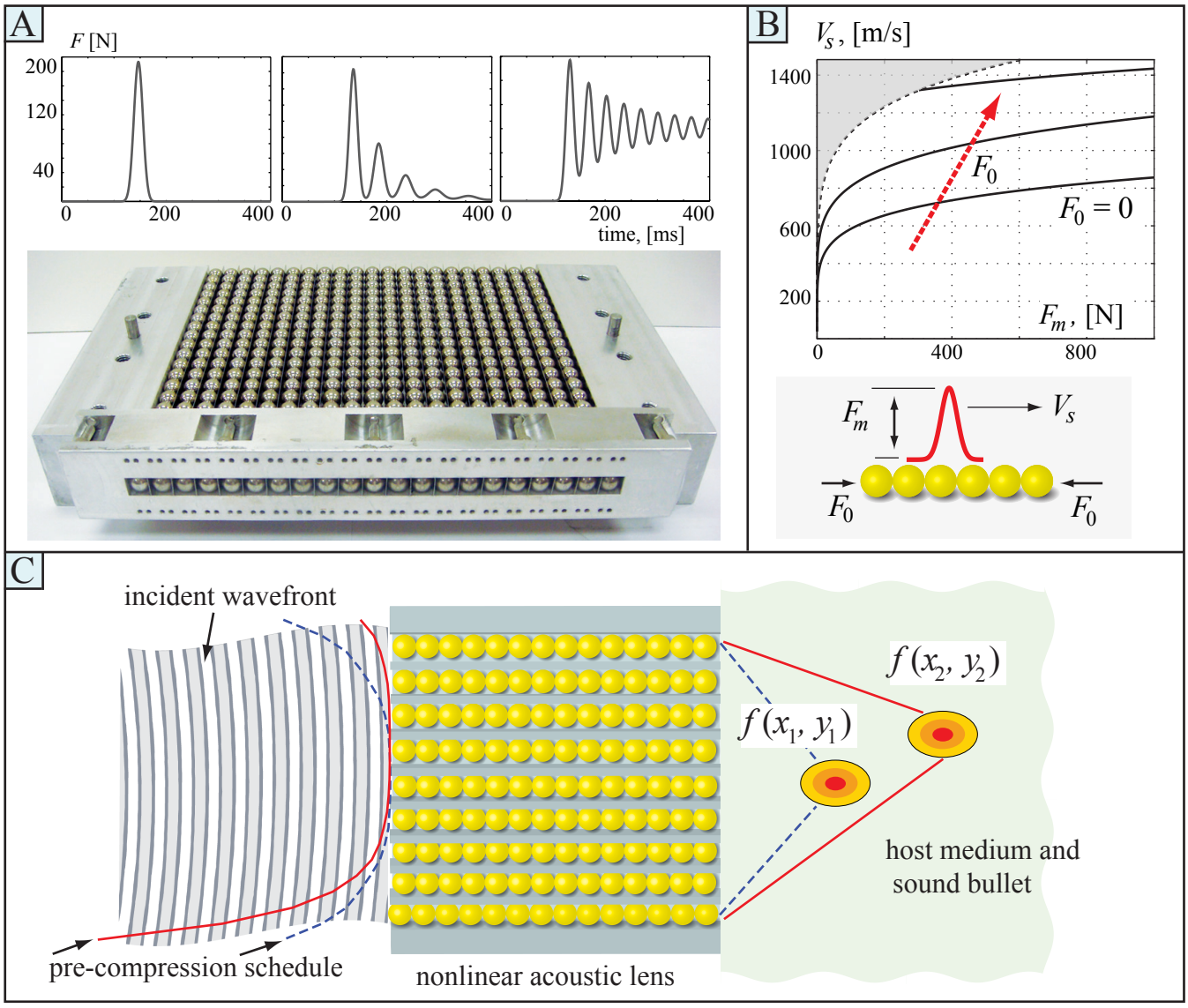

Fig. 1. Nonlinear acoustic lens. **(A)** Prototype consisting of 21 independent chains, each composed of 21 steel spheres and employed as the wave-modulation component (density $\rho = 8100$ Kg/m^3, Young's modulus $E = 196$ GPa, and diameter $D = 9.5$ mm). Numerical simulation of the prototype shows it to be capable of supporting single solitary waves (top left insert), trains of solitary waves (center), and shocks (right). **(B)** The phase velocity V_s of waves with force amplitude F_m traveling in the acoustic lens strongly depends on the initial strain state determined by static pre-compression force F_0. The gray shaded region of the parameter space indicates where the response is weakly nonlinear. **(C)** Because the phase velocity depends on F_0, the distribution of F_0 may be chosen to focus acoustic energy into a "sound bullet". The position of the focus lies on the lens' symmetry axis $f(x_1, y_1)$ when F_0 is symmetric about it (dashed blue line), or off the symmetry axis $f(x_2, y_2)$ when F_0 is asymmetric (solid red line).

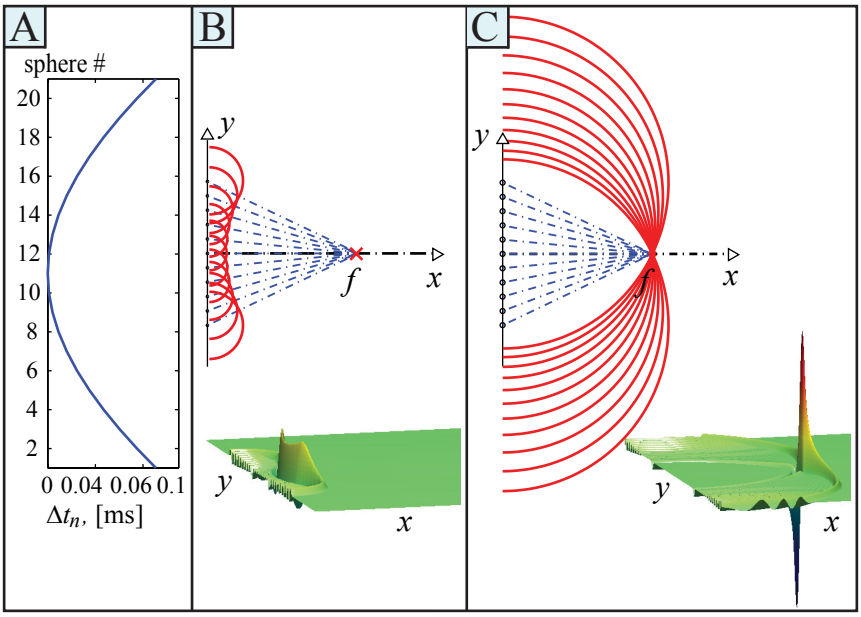

Fig. 2. Results of analytical calculations in support of the lens design. **(A)** Time delay distribution (Eq. [S1]) necessary to obtain a focal point in air at ($x_f = 13$ cm, $y_f = 0$ cm), along the lens' symmetry axis. **(B)** Schematic of the wave field shortly after generation (top, lines of constant phase in red and ray paths in blue), and analytical solution for pressure field (bottom, from Eq. [**3**]). **(C)** Wave field and analytical solution for pressure at a later time, when the acoustic energy coalesces at the focal point. The resulting sound bullet is composed of a symmetric pressure maximum and minimum.

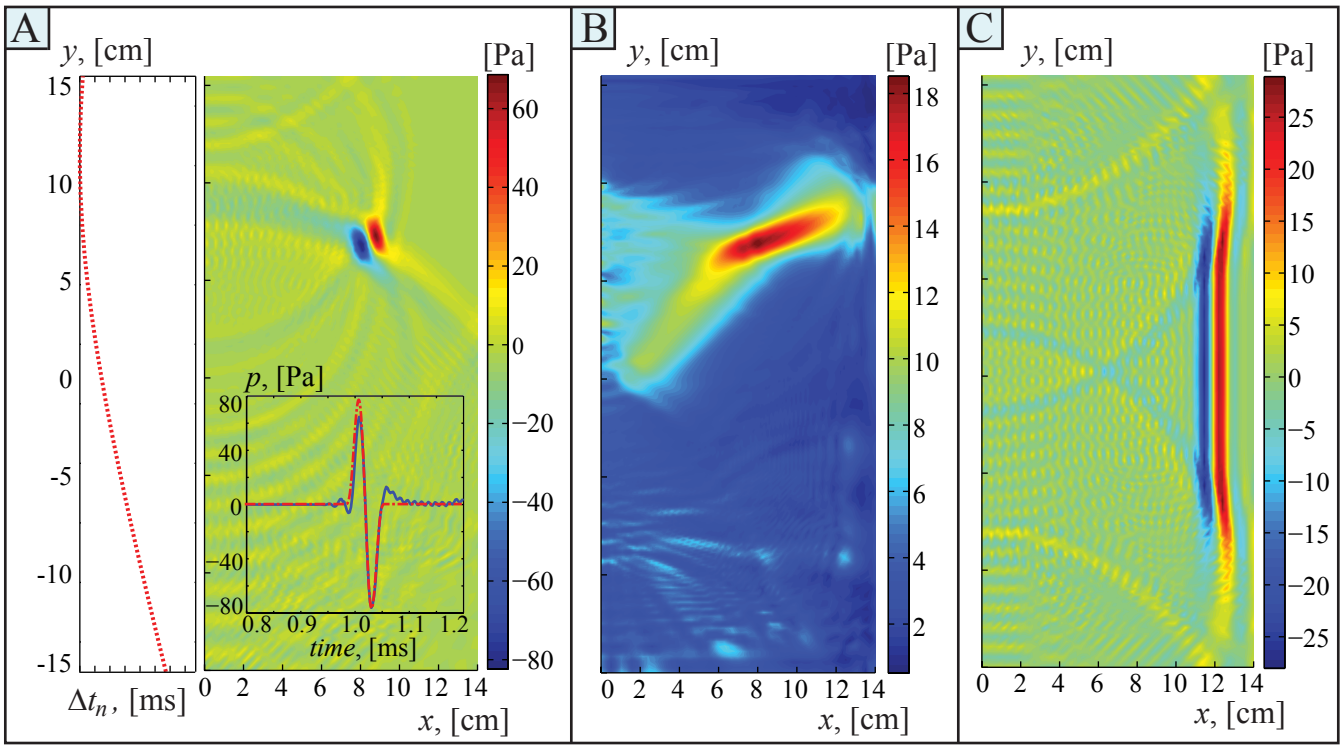

Fig. 3. Results of numerical simulations of the interaction of the lens with air as the host medium. **(A)** A sound bullet away from the lens' symmetry axis results from an asymmetric delay distribution (left inset). The pressure history at the focal point ($x_f = 9$ cm, $y_f = 7$ cm) is shown in the right inset and agrees qualitatively with the analytical prediction (dashed red line, from Eq. [3]). **(B)** The root-mean-square (RMS) pressure field illustrates that the sound bullet can travel finite distances while retaining its compact shape (see the width of the region of large pressure fluctuations). **(C)** A focal point at infinity ($x_f = \infty$ cm, $y_f = 0$ cm), or a traveling compact planar wavefront, can be generated by zero or uniform pre-compression on each chain.

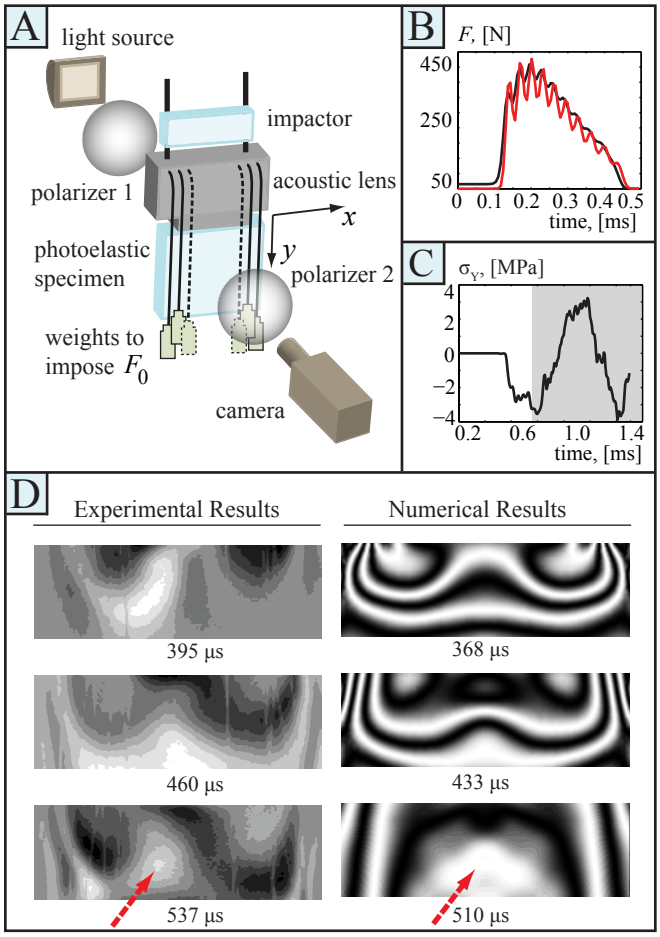

Fig. 4. Comparison of experiments and numerical results. **(A)** Schematic diagram representing the photoelastic experiment carried out to observe stress focusing within a polycarbonate plate. **(B)** The waves within the lens are computed to be shock-like structures due to the large impacting mass used experimentally to generate the input. The red line corresponds to waves in the most compressed chain at the extremes of the lens (1 and 21). The black line indicates waves in the uncompressed chain in the middle of the lens (11). **(C)** The computed stress component σ_y at the focal point shows the coalescing of pressure waves at $t = 0.58$ ms. The area shaded in gray indicates the presence of reflected waves from the bottom portion of the photoelastic plate. **(D)** Experimentally captured photoelastic fringes and equivalent field computed with a FE model provide qualitative agreement. The arrows point to the location of the focal point.